IOP Publishing New J. Phys. 26 (2024) 113009 https://doi.org/10.1088/1367-2630/ad8eea

New Journal of Physics
The open access journal at the forefront of physics

Deutsche Physikalische Gesellschaft DPG
IOP Institute of Physics

Published in partnership with: Deutsche Physikalische Gesellschaft and the Institute of Physics

OPEN ACCESS

RECEIVED
19 July 2024

REVISED
20 October 2024

ACCEPTED FOR PUBLICATION
5 November 2024

PUBLISHED
18 November 2024

PAPER

Continuous-variable electromechanical quantum thermal transistors

Wenjie Nie[1,*], **Junxi Xu**[1], **Huiya Zhan**[1], **Aixi Chen**[2,*] and **Yueheng Lan**[3,*]

[1] Department of Applied Physics, East China Jiaotong University, Nanchang 330013, People's Republic of China
[2] Department of Physics, Zhejiang Sci-Tech University, Hangzhou 310018, People's Republic of China
[3] Department of Physics, Beijing University of Posts and Telecommunications, Beijing 100876, People's Republic of China
[*] Authors to whom any correspondence should be addressed.

E-mail: niewenjiezhu@sina.cn, aixichen@zstu.edu.cn and lanyh@bupt.edu.cn

Keywords: electromechanical, mechanical motion, quantum thermal transistor, optomechanical coupling, precision measurements

Abstract

We present a scheme to realize quantum thermal transistor effects in a continuous-variable electromechanical system including two microwave cavities and one mechanical oscillator. The thermal noise fluxes between the quantum system and its baths are evaluated by quantum master equation. It is shown that the thermal noise flux at one microwave cavity as an emitter can be dissipated into the other as a collector by combining the heating Stokes and cooling anti-Stokes processes. The indirect energy transfers between the two microwave modes can be significantly amplified by small energy changes at the mechanical oscillator as the base. The extremely high amplification depends sensitively on the detunings of the two microwave modes, which provides a new tool for precision measurements. This study opens the door for constructing quantum thermal transistors using various continuous-variable systems and is well accessible based on current experimental techniques.

1. Introduction

In recent years, rapid progress has been made in the thermal noise energy harvesting and rectification at the nanoscale [1–3], resulting in unique applications in the implementation of quantum heat engines [4–6], quantum thermal diodes [7, 8] and transistors [9, 10] in nanosystems. The main components of such systems typically include thermal rectifiers, such as qubit and qutrit [11–14], spins [7, 8, 15–17], quantum dots [18] or superconducting circuits [19], which are usually simplified as two-level or three-level systems [20–22] and designed to bias the heat flow in a given direction [3]. These quantum subsystems are also coupled to two or more external heat sources simultaneously [7, 9, 22, 23], so that the control of heat flow is the result of a combined action of external temperature bias and the internal energy levels and coupling control. In addition, the regulation of heat flow and transistor effects can be achieved by driving two-level systems with an external optical field [24, 25].

Previous researches on quantum thermal transistors (QTTs) have mainly focused on spin-boson models, where the level spacing and transitions as well as the couplings between subsystems need to be designed extremely carefully [26–28]. Further, these quantum thermal regulation typically occurs in nanoscale systems with finitely many levels, while similar research at the macroscopic scales is still lacking, which makes it urgent to investigate whether a three-terminal QTT can be realized in mesoscopic or even macroscopic systems, such as continuous-variable (CV) systems [29–31]. It is noted that the CV optomechanical system provides a novel platform for exploring macroscopic quantum thermal transport, such as permanent directional heat currents [32], quantum heat management [33–36], nonreciprocal heat transport [37], topological energy transfer [38], optomechanical heat engine [39, 40] and geometric thermo-phonon exchange [41]. In this letter, we demonstrate that a QTT can be created with a CV electromechanical system, made of two microwave cavities and one mechanical oscillator. It is shown that a quantum thermal noise flux can be established between the mechanical oscillator and its baths, and the temperature of the mechanical

end can be used to regulate the noise fluxes at the two microwave components of the system. Further, we also show that the amplification of the noise fluxes is highly sensitive to the microwave cavity parameters, which may be used in precision measurement.

The rest of the paper is structured as follows. In section 2, we describe the system model and derive the general expressions of the thermal noise fluxes between the system and its baths using the quantum master equation method. In section 3 we focus on achieving the thermal transistor effect by regulating the amplitude and direction of the thermal noise fluxes in the system. Further, we analyze in detail the influence of the system parameters on the amplification factors of the noise fluxes and the quantum Fisher information, which quantifies the sensitivity of the system to unknown parameters. The section 4 is a brief summary of the article.

2. Model and dynamics

As sketched in figure 1(a), we consider a typical model of a three-mode electromechanical system including two microwave cavities and one mechanical oscillator, where the phonon mode a_m with frequency ω_m is simultaneously coupled to the two microwave photon modes a_1 and a_2 with frequencies ω_{a1} and ω_{a2} [31, 42–45]. The realization of such a system can be resorted to two lumped-element superconducting circuits and one intermediate mechanical oscillator [44–47], where the microwave cavities are driven by external microwave sources with frequencies ω_{01} and ω_{02}, as shown in figure 1(b). The total Hamiltonian in the interaction picture with respect to $H_0 = \hbar\omega_{a1}a_1^\dagger a_1 + \hbar\omega_{a2}a_2^\dagger a_2$ is given by [29, 31, 44]

$$\frac{H}{\hbar} = \omega_m a_m^\dagger a_m + \sum_{j=1,2} a_j^\dagger a_j \left[\Delta_{0j} - g_j\left(a_m^\dagger + a_m\right)\right] + i\Omega_j\left(a_j^\dagger - a_j\right), \tag{1}$$

where $\Delta_{0j} = \omega_{aj} - \omega_{0j}$ and $\left|\Omega_j\right| = \sqrt{2P_j\kappa_j/(\hbar\omega_{0j})}$ with P_j and κ_j being the driving power and decay rate of the cavity field j, respectively. g_j denotes the electromechanical coupling strength between the mechanical mode and the microwave mode j.

When the microwave cavities are intensely driven, we decompose each operator into the steady-state average and a small quantum fluctuation, i.e. $a_\mu = a_{\mu s} + \delta a_\mu$ with $\mu = 1, 2, m$. The steady-state values are obtained by setting the time evolution of operators in equation (1) to zero, getting $a_{js} = \Omega_j/(i\Delta_j + \kappa_j)$ and $a_{ms} = (ig_1|a_{1s}|^2 + ig_2|a_{2s}|^2)/(i\omega_m + \kappa_m)$, where $\Delta_j = \Delta_{0j} - g_j(a_{ms}^* + a_{ms})$ describes the effective detuning and κ_m is the mechanical damping rate. The linear quantum Langevin equations (QLEs) for the quantum fluctuations are given by

$$\begin{aligned}
\delta\dot{a}_m &= i\sum_j G_j\left(\delta a_j^\dagger + \delta a_j\right) - \left(i\omega_m + \kappa_m\right)\delta a_m + \sqrt{2\kappa_m}a_m^{in},\\
\delta\dot{a}_1 &= iG_1\left(\delta a_m^\dagger + \delta a_m\right) - \left(i\Delta_1 + \kappa_1\right)\delta a_1 + \sqrt{2\kappa_1}a_1^{in},\\
\delta\dot{a}_2 &= iG_2\left(\delta a_m^\dagger + \delta a_m\right) - \left(i\Delta_2 + \kappa_2\right)\delta a_2 + \sqrt{2\kappa_2}a_2^{in},
\end{aligned} \tag{2}$$

where $G_j = g_j a_{js}$ with a_{js} being assumed to be real and positive [44]. a_1^{in}, a_2^{in} and a_m^{in} are the vacuum and thermal input noise operators with zero mean value, with the following correlation [48]: $\langle a_\mu^{in}(t)a_\mu^{in,\dagger}(t')\rangle = [N_\mu(\omega_\mu)+1]\delta(t-t')$ and $\langle a_\mu^{in,\dagger}(t)a_\mu^{in}(t')\rangle = N_\mu(\omega_\mu)\delta(t-t')$ with $N_\mu(\omega_\mu) = \exp(\frac{\hbar\omega_\mu}{k_B T_\mu} - 1)^{-1}$. k_B is the Boltzmann constant and T_μ is the temperature of the thermal bath μ, as shown in figure 1(a). The linearized Hamiltonian reads $H_L/\hbar = \omega_m\delta a_m^\dagger\delta a_m + \sum_j \Delta_j\delta a_j^\dagger\delta a_j$ $-G_j(\delta a_j^\dagger + \delta a_j)(\delta a_m^\dagger + \delta a_m)$ and the corresponding level diagram and the typical transition routes are shown in figure 1(c).

It is clearly seen from equation (2) that noise accounts for the energy transfer between subsystems and their baths, i.e. $Q_m(t) = \hbar\omega_m\langle\int[\xi_p(t) - \kappa_m\delta p(t)]\delta p(t)\mathrm{d}t\rangle$ being the stochastic energy induced by the noise $\xi_p = i(a_m^{in,\dagger} - a_m^{in})/\sqrt{2}$ on the momentum quadrature of the oscillator $\delta p = i(\delta a_m^\dagger - \delta a_m)/\sqrt{2}$ [49–51]. In order to explore the possible QTT effect, here we use the quantum master equations (QMEs) to evaluate the thermal noise flux J_μ between the subsystem μ and its bath. With the linearized Hamiltonian H_L, the QMEs describing the evolution of the density matrix of the system reads [48]

$$\dot{\rho} = \frac{i}{\hbar}\left[\rho, H_L\right] + \mathcal{L}_1\left[\rho\right] + \mathcal{L}_2\left[\rho\right] + \mathcal{L}_m\left[\rho\right], \tag{3}$$

where $\mathcal{L}_\mu[\rho] = \kappa_\mu(N_\mu+1)\mathcal{D}[a_\mu]\rho + \kappa_\mu N_\mu\mathcal{D}[a_\mu^\dagger]\rho$ are the Liouville super-operators of the microwave and mechanical baths. $\mathcal{D}[a_\mu]\rho = 2a_\mu\rho a_\mu^\dagger - a_\mu^\dagger a_\mu\rho - \rho a_\mu^\dagger a_\mu$ is the standard dissipative Lindblad term. The thermal noise fluxes in and out of a quantum system are related to the temporal variation of the system mean

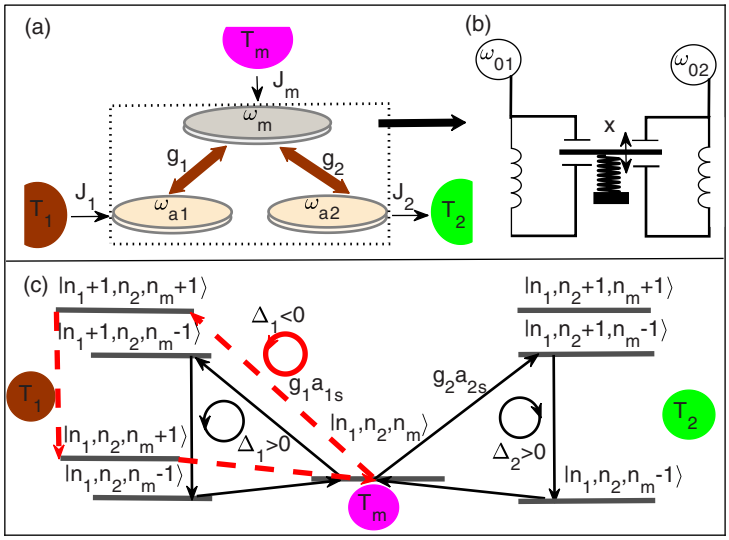

Figure 1. (a) Schematic illustration of a three-mode electromechanical system with two microwave modes and one mechanical mode. Each subsystem is in contact with its thermal environment at a certain temperature. (b) A specific realization of the system with two lumped-element superconducting circuits and one intermediate mechanical oscillator. (c) Level diagram of the linearized Hamiltonian $H_{\rm L}$. n_1, n_2, n_m denotes the state of n_1 and n_2 photons and n_m phonons in the displaced frame. Black (red) ↻ denotes the transitions paths corresponding to the anti-Stokes (Stokes) process with $\Delta_{1,2} > 0$ ($\Delta_1 < 0$). By manipulating the left and right cavities in the blue- and red-detuning regions respectively, a complete cyclic transition path through the connection of the anti-Stokes and the Stokes transition processes $|n_1+1, n_2, n_m+1\rangle \to |n_1, n_2, n_m+1\rangle \to |n_1, n_2, n_m\rangle \to |n_1, n_2+1, n_m-1\rangle \to |n_1, n_2, n_m-1\rangle \to |n_1, n_2, n_m\rangle \to |n_1+1, n_2, n_m+1\rangle$, called the red ↻ plus black ↻ path, can be established, which leads to that the energy absorbed by the microwave cavity 1 from the left thermal bath can significantly compensate for the energy transferred from the microwave cavity 2 to the right thermal bath. This indirect energy transfer through the mechanical end acting as an intermediary is responsible for the realization of the QTT.

energy, i.e. $\sum_\mu J_\mu = \partial\langle H_{\rm L}\rangle/\partial t$ [52]. Then, one can identify the noise flux J_μ as $J_\mu = Tr(\mathcal{L}_\mu[\rho]H_{\rm L})$ [9], which are calculated by using the QMEs (3) as

$$\begin{aligned} J_m &= \hbar\kappa_m\left[2\omega_m\left(N_m - \langle\delta a_m^\dagger \delta a_m\rangle\right) + G_1M_1 + G_2M_2\right], \\ J_1 &= \hbar\kappa_1\left[2\Delta_1\left(N_1 - \langle\delta a_1^\dagger \delta a_1\rangle\right) + G_1M_1\right], \\ J_2 &= \hbar\kappa_2\left[2\Delta_2\left(N_2 - \langle\delta a_2^\dagger \delta a_2\rangle\right) + G_2M_2\right], \end{aligned} \tag{4}$$

where $M_j = \langle(\delta a_j^\dagger + \delta a_j)(\delta a_m^\dagger + \delta a_m)\rangle$. It is evident that each noise flux in equation (4) consists of three parts, which are proportional to the thermal photon or phonon numbers N_μ, the average occupancy $\overline{N}_\mu = \langle\delta a_\mu^\dagger \delta a_\mu\rangle$ and the second moments M_j, respectively. In particular, for any linearly coupled CV systems with multiple harmonic oscillators, the noise flux between each subsystem and its corresponding bath can be straightforwardly generalized as $J_n = \hbar\kappa_n[2E_n(N_n - \overline{N}_n) + \sum_n G_{\{n\}}M_{\{n\}}]$, where $n(n = 1, 2, 3, \ldots)$ is the number of the harmonic oscillators, E_n and $\{n\}$ denotes the effective energy and the coupling strategy of subsystems, respectively. In the steady state of $\dot{\rho} = 0$, we have $J_1 + J_2 + J_m = 0$, which corresponds to the energy conservation of the system. The fluxes can be measured by the scale of $\hbar\omega_m$, i.e. $J_\mu = J_{0\mu}\hbar\omega_m$ with $J_{0\mu}$ being regarded as a noise particle flux [41]. We emphasize that when a control parameter of the system changes so that the coupled system transitions from one steady state to another, the sum of the changes in noise fluxes at the three ports is always zero, i.e. $\partial J_1 + \partial J_2 + \partial J_m = 0$. This also means that when the noise flux of one of the ports changes, the noise fluxes of the other two ends will also change accordingly, so as to achieve the thermal regulation effects of one flux controlling the other flux.

In the following, we evaluate in detail the moments in equation (4). One approach is to derive the time evolution of all the independent second-order moments, such as $\langle\delta a_1^\dagger \delta a_1\rangle$, $\langle\delta a_2^\dagger \delta a_2\rangle$, $\langle\delta a_m^\dagger \delta a_m\rangle$ and so on, using the quantum master equation (3) and then calculate the steady state dynamics of the moments [41]. Here, we directly solve QLEs (2) to obtain the corresponding steady-state correlation matrix, thus obtaining the second-order moments in the equation (4). For the convenience of calculation, we introduce the quantum fluctuation quadratures of the cavity fields and mechanical oscillator as $x_\mu(t) = (\delta a_\mu^\dagger + \delta a_\mu)/\sqrt{2}$ and $y_\mu(t) = i(\delta a_\mu^\dagger - \delta a_\mu)/\sqrt{2}$. The corresponding input noise quadratures can be defined in the same way. Further, by introducing the vectors of quadratures $f^T(t) = [x_1, y_1, x_2, y_2, x_m, y_m]$ and the corresponding vectors of noises $n^T(t) = \sqrt{2}[\sqrt{\kappa_1}x_1^{in}, \sqrt{\kappa_1}y_1^{in}, \sqrt{\kappa_2}x_2^{in}, \sqrt{\kappa_2}y_2^{in}, \sqrt{\kappa_m}x_m^{in}, \sqrt{\kappa_m}y_m^{in}]$, the linear QLEs (2) can be

written in the matrix form: $\dot{f}(t) = Af(t) + n(t)$, where A is the drift matrix, given by

$$A = \begin{pmatrix} -\kappa_1 & \Delta_1 & 0 & 0 & 0 & 0 \\ -\Delta_1 & -\kappa_1 & 0 & 0 & 2G_1 & 0 \\ 0 & 0 & -\kappa_2 & \Delta_2 & 0 & 0 \\ 0 & 0 & -\Delta_2 & -\kappa_2 & 2G_2 & 0 \\ 0 & 0 & 0 & 0 & -\kappa_m & \omega_m \\ 2G_1 & 0 & 2G_2 & 0 & -\omega_m & -\kappa_m \end{pmatrix}. \tag{5}$$

When the stability condition of the system is satisfied [53–55], the steady state is a zero-mean Gaussian state and fully characterized by a 6×6 covariance matrix U, defined as $U_{ij} = \langle f_i(\infty) f_j(\infty) + f_j(\infty) f_i(\infty) \rangle / 2$ with $i, j = 1, 2, 3, 4, 5, 6$, which is obtained straightforwardly by solving the Lyapunov equation [56]:

$$AU + UA^T = -D, \tag{6}$$

where $D = \mathrm{diag}[\kappa_1(2N_1+1), \kappa_1(2N_1+1), \kappa_2(2N_2+1), \kappa_2(2N_2+1), \kappa_m(2N_m+1), \kappa_m(2N_m+1)]$. In terms of the covariance matrix U, the steady-state average occupancies in equation (4) are, respectively, $\langle \delta a_m^\dagger \delta a_m \rangle = (U_{55} + U_{66} - 1)/2$, $\langle \delta a_1^\dagger \delta a_1 \rangle = (U_{11} + U_{22} - 1)/2$ and $\langle \delta a_2^\dagger \delta a_2 \rangle = (U_{33} + U_{44} - 1)/2$. Similarly, the moments M_1 and M_2 are, respectively, $M_1 = 2U_{15}$ and $M_2 = 2U_{35}$.

3. Thermal transistor effects

Figures 2(a) and (b) show the noise fluxes J_{01}, J_{02} and J_{0m} as a function of the normalized detuning Δ/κ at $\Delta_2 = \Delta_1 = \Delta$ and $\Delta_2 = -\Delta_1 = \Delta$. We assume that the system works in the resolvable sideband region of $\kappa_j \ll \omega_m$, i.e. $\omega_m/2\pi = 10$ MHz and $\kappa_j = 0.03\omega_m$. It is also noted that in general the mechanical oscillator is very thermally dense because of the two associated microwave cavities. Thus, the mechanical oscillator must be pre-cooled by lowering the environment temperatures of the thermal bath, i.e. $T_m = 300$ mK. We see from figure 2(a) that $J_{01} = J_{02} < 0$ and therefore the system dissipates energy into two microwave baths through the cooling anti-Stokes process, i.e. the cooling transition paths marked by the black ↺ and ↻ in figure 1(c) [41, 57–59]. At the same time, we also see that the system absorbs the same amount of energy from the mechanical bath to ensure that energy conservation in the steady state holds true, i.e. $J_{0m} = -2J_{0j}$. In this case, no matter how a single external parameter changes, we always have $\partial J_1/\partial J_m = -1/2$ and $\partial J_2/\partial J_m = -1/2$. Obviously, the system can not exhibit the amplified flow regulation effect similar to that of an electrical transistor [60–62] due to the uniform dissipation of the absorbed energy, as shown in figure 2(c). We stress that in the case of the resolvable sideband the mechanical oscillator can be further cooled, i.e. the average occupancy $\langle \delta a_m^\dagger \delta a_m \rangle \ll N_m$, because both cooling anti-Stokes processes reduce the effective energy of the mechanical mode through the dissipation channels in the cavity fields.

To achieve thermal transistor regulation effects, we reverse one of the dissipative fluxes, e.g. J_{01}, by reversing the corresponding detuning Δ_1. At this time, the heating Stokes process is expected to dominate the dynamics of the subsystem composed of the mechanical oscillator and the microwave mode 1, which leads to that the system absorbs energy from the microwave bath 1. We also see clearly from figure 2(b) that when the reverse operation of the left microwave cavity is in the blue-detuning regime with $\Delta_1 < 0$, J_{01} is indeed reversed to positive and the energy transfers from the microwave bath 1 to the mechanical oscillator. In particular, in the presence of the right cooling Stokes process with the detunging $\Delta_2 > 0$, the two combined processes lead to that the energy absorbed from the microwave thermal bath 1 can immediately compensate for the energy dissipated into the second microwave thermal bath, that is, $J_{02} \approx -J_{01}$, as shown in figures 2(b) and (d). From the perspective of energy level transition, the indirect energy transfer is achieved via the combined cyclic transition path mediated by the mechanical oscillator, i.e. the red ↺ plus black ↻ path in figure 1(c). That is, along this cyclic path, the energy absorbed from the microwave bath 1 by the blue-detuning transitions $|n_1, n_2, n_m\rangle \to |n_1+1, n_2, n_m+1\rangle \to |n_1, n_2, n_m+1\rangle$ can be significantly dissipated into the microwave bath 2 by the other red-detuning transitions $|n_1, n_2, n_m\rangle \to |n_1, n_2 +1, n_m-1\rangle \to |n_1, n_2, n_m-1\rangle$. Correspondingly, the net flux J_{0m} in the cyclic path is greatly reduced by the opposite transitions $|n_1, n_2, n_m \pm 1\rangle \to |n_1, n_2, n_m\rangle$, i.e. $|J_{0m}| \ll |J_{0j}|$, as shown in the inset of figure 2(b). Clearly, the quantum noise transport is used to establish the opposite transitions at the mechanical end and further mediate the energy transfer from one microwave end to another along the cyclic path.

Furthermore, the changes of the transition rates of $|n_1, n_2, n_m \pm 1\rangle \to |n_1, n_2, n_m\rangle$ will influence the probability of the cyclic path so that the energy transfer between the two microwave ends can be controlled by the mechanical bath. For example, when T_1 and T_2 ($T_1 > T_2$) are fixed, the increase of T_m reduces the transition rate ρ^+ of the phonon dissipation $|n_1, n_2, n_m+1\rangle \to |n_1, n_2, n_m\rangle$ but enhances the rate ρ^- of the opposite phonon absorption $|n_1, n_2, n_m-1\rangle \to |n_1, n_2, n_m\rangle$, where we usually have $\rho^+ > \rho^-$. Although the

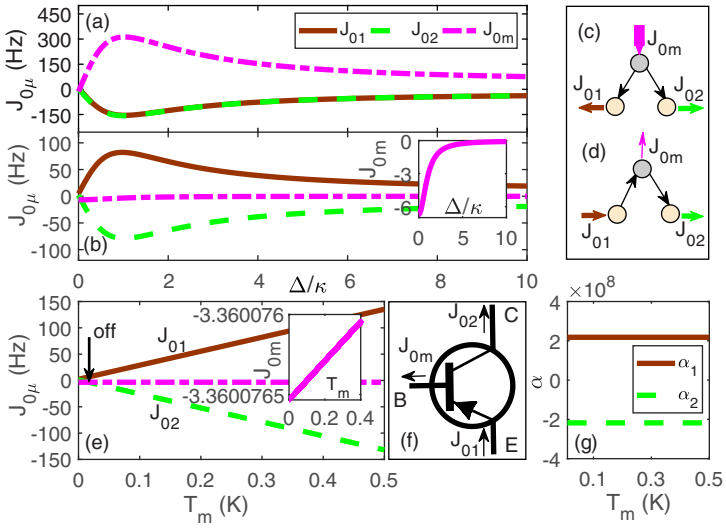

Figure 2. $J_{0\mu}$ as a function of Δ/κ with (a) $\Delta_2 = \Delta_1 = \Delta$ and (b) $\Delta_2 = -\Delta_1 = \Delta$. (c) and (d) Directions of $J_{0\mu}$. (e) $J_{0\mu}$ and (g) α_1 and α_2 as a function of T_m with $\Delta_2 = -\Delta_1 = \kappa$ with $\kappa_j = \kappa$ and (f) schematic diagram of the electromechanical system as a thermal transistor. Insets: Magnification of J_{0m}. We select the feasible experimental parameters [46], i.e. $\omega_m/2\pi = 10$ MHz and $\kappa_m/2\pi = 100$ Hz. The other microwave parameters are assumed to be the same, i.e. $\omega_{0j}/2\pi = 10.1$ GHz, $P_j = 0.05$ μW, $\kappa_j = 0.03\omega_m$ and $g_j/2\pi = 0.08$ Hz. The temperatures $T_1 = 500$ mK, $T_2 = 10$ mK and $T_m = 300$ mK.

two transition rates vary inversely with T_m, their joint transition rate $\rho^+\rho^-$ can still increase with the increase of T_m. Then, the probability of the complete cyclic path increases with the increase of T_m so that the energy transfers J_{01} and J_{02} increases with increasing T_m. Consequently, we can use the mediated temperature T_m as a gating parameter to regulate the fluxes at the other microwave ends, i.e. J_{01} and J_{02}. Note that in the modulation process the flux $|J_{0m}| \ll |J_{01,02}|$ is required to ensure the amplification of flux in the system.

In figure 2(e), we demonstrate the temperature regulatory effects of fluxes by depicting $J_{0\mu}$ as a function of T_m. We see from figure 2(e) that when T_m is sufficiently low, all three noise fluxes are suppressed, even giving $J_{02} = 0$ at $T_m = 3.8$ mK. Therefore, the system is at the off state. When T_m increases continuously beyond a threshold value with $|J_{02}| \simeq |J_{0m}|$, the amplitudes of J_{01} and J_{02} increase quickly with T_m, while the amplitude of J_{0m} remains much lower than J_{01} and J_{02} and decreases slightly with T_m. At this time, the modulated system switches to the on state and a tiny change of J_{0m} will cause giant changes of J_{01} and J_{02}, thereby achieving the amplification of the fluxes. It should be emphasized that the combination of the Stokes and anti-Stokes processes breaks the symmetry of quantum transition paths, which constitutes a prerequisite condition for a directionality of the noise fluxes of the thermal transistor, where the microwave cavity ends 1 and 2 are regarded as the emitter (E) and the collector (C), respectively, as shown in figure 2(f). In particular, similar to an electrical transistor [60–62], the source and drain noise fluxes J_{01} and $-J_{02}$ in the current system can be modulated, switched on or off and amplified by the gate parameter T_m at the mechanical end which serves as the base (B).

In order to evaluate the amplification properties of the system, we adopt a dynamical amplification factor [9, 10, 12]

$$\alpha_{1,2} = \frac{\partial J_{1,2}}{\partial J_m}, \tag{7}$$

which is a measure of the thermal transistor ability to amplify a small variation of the noise flux at the base (B) and can be casted as $\alpha_{1,2} = (\partial J_{1,2}/\partial T_m)(\partial J_m/\partial T_m)^{-1}$ when the gate temperature T_m is changed. Correspondingly, if a small change in J_m makes a large change in J_1 or J_2, the factor $\alpha_{1,2}$ will be larger than 1, i.e. $|\alpha_{1,2}| > 1$, and the thermal transistor effect of the system will be observed. Further, the larger the amplification factor is, the better the thermal amplification function of the system is. In figure 2(g), we plot the amplification factors α_1 and α_2 as a function of T_m. It is found from figure 2(g) that the amplification factors of J_{01} and J_{02} are almost constant and very huge, i.e. $|\alpha_2| \approx \alpha_1 \approx 2.18 \times 10^8$, which exhibits a strong robustness to noise strengths. This also derives from the fact that when the system works at $\Delta_2 = -\Delta_1$, the mechanical mode cannot be cooled or heated significantly so that $\langle \delta a_m^\dagger \delta a_m \rangle \approx N_m$, which leads to a very small and slightly temperature-dependent flux J_{0m} in equation (4). In contrast, N_1 and N_2 are constants but $\langle \delta a_1^\dagger \delta a_1 \rangle$ and $\langle \delta a_2^\dagger \delta a_2 \rangle$ always vary with T_m. Consequently, J_{01} and J_{02} in equation (4) depend significantly on T_m so that the ratio of two slopes, i.e. $\alpha_{1,2} = (\partial J_{1,2}/\partial T_m)(\partial J_m/\partial T_m)^{-1}$ can be very large. Therefore, the

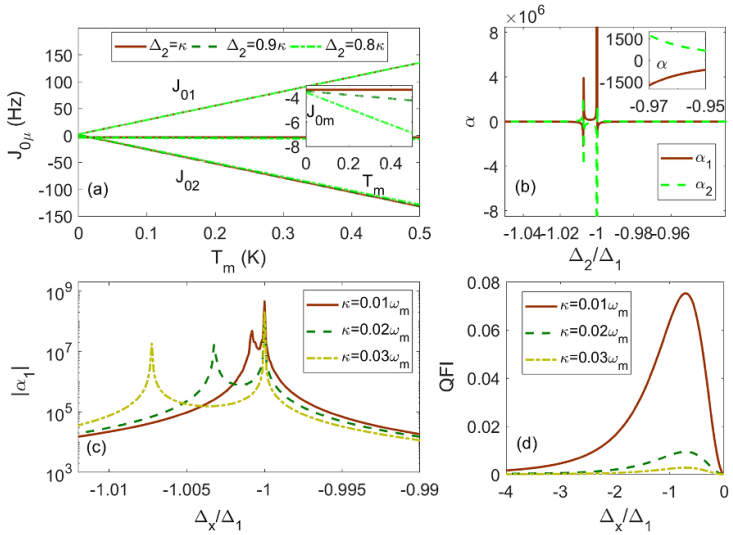

Figure 3. (a) J_{01}, J_{02} and J_{0m} as functions of T_m with different Δ_2 at $\Delta_1 = -\kappa$. (b) α_1 and α_2 as functions of Δ_2/Δ_1 and (c) $|\alpha_1|$ as a function of Δ_x/Δ_1 at $\Delta_1 = -\kappa$. (d) $\mathcal{F}$ as a function of the unknown parameter Δ_x/Δ_1 for different κ. Other parameter values are the same as those in figure 2. Insets: magnification of J_{0m} and α.

current setup provides a simple and effective way of inducing large-amplitude changes in energy transport at the microwave end with a tiny variation at the mechanical end, thereby realizing the QTT.

The changes of the noise fluxes as a function of T_m with different Δ_2 are shown in figure 3(a). We see from figure 3(a) that J_{01} keeps constant and J_{02} changes slightly with decreasing Δ_2 at a given T_m. However, the amplitude of J_{0m} increases significantly with a decrease of Δ_2, as shown in the inset of figure 3(a). This is because when $\Delta_2 < -\Delta_1$, the absorbed noise flux from bath 1 rapidly exceeds the dissipative noise flux entering bath 2 so that more redundant energy should dissipate into the mechanical bath. In figure 3(b) we depict the amplification factors α_1 and α_2 as functions of Δ_2/Δ_1. We found that an extremely high amplification can be always obtained, i.e. $\alpha_1 = -671.6$ and $\alpha_2 = 670.6$ as $\Delta_2 = 0.95\kappa$, as shown in the inset of figure 3(b). It is noted that the huge amplification factors α_1 and α_2 appear at two particular detunings Δ_2 for which J_{0m} is 0 and the energy absorbed from left thermal bath completely compensate for the energy transferred to right one. This occurs for $\Delta_2 \simeq -\Delta_1$ and $\Delta_2 \simeq -1.007\Delta_1$, and there exists a minimum value of amplification factor between the two. Therefore, the amplification factors drop quickly and depend sensitively on the detuning ratio.

In particular, the sensitivity of the amplification can be used in a high-precision measurement of control parameters [63]. For example, when a parameter, such as $\Delta_2 \approx \Delta_{02} = \Delta_x$, is unknown, we can adjust the known parameter Δ_1 to change until a certain criteria is reached, which corresponds to an extreme amplification, thereby determining this unknown parameter and achieving alignments of two microwave driving frequencies. In figure 3(c) we depict $|\alpha_1|$ as a function of Δ_x/Δ_1 at different κ's. We see from figure 3(c) that the width between two extreme amplification points increases with increasing κ. Therefore, the smaller κ, the higher sensitivity to Δ_x. Furthermore, we can use quantum Fisher information (QFI) to quantify the sensitivity of the system to Δ_x (see figure 3(d)), which for a CV Gaussian state, is [64–67]

$$\mathcal{F} = 2\mathrm{vec}\left[\partial_x U\right]^{\dagger} \mathcal{M}^{-1} \mathrm{vec}\left[\partial_x U\right] + \partial_x \mathbf{R}_s^{\mathrm{T}} U^{-1} \partial_x \mathbf{R}_s, \tag{8}$$

where $\mathcal{M} = 4U^{\dagger} \otimes U + \Xi \otimes \Xi$ with $\Xi = \Lambda \oplus \Lambda \oplus \Lambda$ and $\Lambda = [0, 1; -1, 0]$; vec[•] denotes the vectorization of a matrix and ∂_x denotes the derivation with respect to the parameter x; $\mathbf{R}_s$ is the vector of average values of $f(t)$. The ultimate limit in precision is given by the Cramér-Rao bound $\mathrm{Var}(\Delta_x) \geqslant 1/(\mathcal{N}\mathcal{F})$ with $\mathcal{N}$ being the number of independent probes [67]. Comparing figures 3(c) and (d), we see that the largest QFI is obtained in the region near $\Delta_x = -\Delta_1$ which overlaps with that for the extreme amplification in J_{01}. Clearly, in the selected parameter range a small decay rate κ significantly enhances QFI, thereby indeed improving measurement precision.

Finally, we remark that in experiments, the mechanical oscillator can be coupled capacitively to two identical superconducting microwave circuits [45–47], where the coupling strength g_j is related to the parameters of the capacitor and the mechanical oscillator and can easily reach the order of 1 Hz. Further, the noise fluxes can be experimentally demonstrated by detecting the covariance matrix U, where the second-order moments of the microwave modes can be acquired via the homodyne detection of the output

field [68] and the detection of the second moments for the mechanical mode can be obtained by constructing auxiliary cavity [56]. In addition, the QTT can quickly switch between on and off states by controlling the external driving, which determines the amplitude of each noise flux.

4. Conclusions

We have proposed an experimentally feasible microwave electromechanical scheme to realize continuous-variable quantum thermal transistor. We found that by combining the heating Stokes and cooling anti-Stokes processes of the system, the tiny changes of the energy transfer between the mechanical oscillator and the bath produce amplified variations in energy transport at the microwave ends. In particular, the amplifications of the noise fluxes can be sensitively modulated by changing the relative detunings of the two microwave cavities. As a future direction, it would be interesting to study the quantum thermal transistor effects and related quantum precision metrology based on various continuous-variable electromechanical [31, 45], optomechanical [29, 69, 70] or magnomechanical systems [67, 71, 72], as well as to explore the influence of the memory effect of the non-Markovian environment on the thermal transfer and the quantum Fisher information of the coupled system [73–75].

Data availability statement

All data that support the findings of this study are included within the article (and any supplementary files).

Acknowledgments

This work is supported by the National Natural Science Foundation of China (NSFC) under Grants Nos. 12065008, 12175199, 12375030 and 12464048, the Natural Science Foundation of Jiangxi Porvince under Grant No. 20224BAB201026 and the Foundation of Department of Scicence and Technology of Zhejiang Province under Grant No. 2022R52047.

ORCID iD

Aixi Chen https://orcid.org/0000-0002-7953-3752

References

[1] Li N, Ren J, Wang L, Zhang G, Hänggi P and Li B 2012 *Colloquium*: Phononics: manipulating heat flow with electronic analogs and beyond *Rev. Mod. Phys.* **84** 1045
[2] Benenti G, Casati G, Saito K and Whitney R S 2017 Fundamental aspects of steady-state conversion of heat to work at the nanoscale *Phys. Rep.* **694** 1
[3] Landi G T, Poletti D and Schaller G 2022 Nonequilibrium boundary-driven quantum systems: models, methods and properties *Rev. Mod. Phys.* **94** 045006
[4] Quan H T, Liu Y-X, Sun C P and Nori F 2007 Quantum thermodynamic cycles and quantum heat engines *Phys. Rev.* E **76** 031105
[5] Ono K, Shevchenko S N, Mori T, Moriyama S and Nori F 2020 Analog of a quantum heat engine using a single-spin qubit *Phys. Rev. Lett.* **125** 166802
[6] Xiao Y, Liu D, He J, Ma Y, Wu Z and Wang J 2023 Quantum Otto engine with quantum correlations *Phys. Rev.* A **108** 042614
[7] Yan Y, Wu C-Q and Li B 2009 Control of heat transport in quantum spin systems *Phys. Rev.* B **79** 014207
[8] Balachandran V, Benenti G, Pereira E, Casati G and Poletti D 2018 Perfect diode in quantum spin chains *Phys. Rev. Lett.* **120** 200603
[9] Joulain K, Drevillon J, Ezzahri Y and Ordonez-Miranda J 2016 Quantum thermal transistor *Phys. Rev. Lett.* **116** 200601
[10] Mandarino A, Joulain K, Gómez M D and Bellomo B 2021 Thermal transistor effect in quantum systems *Phys. Rev. Appl.* **16** 034026
[11] Iorio A, Strambini E, Haack G, Campisi M and Giazotto F 2021 Photonic heat rectification in a system of coupled qubits *Phys. Rev. Appl.* **15** 054050
[12] Guo B, Liu T and Yu C 2019 Multifunctional quantum thermal device utilizing three qubits *Phys. Rev.* E **99** 032112
[13] Guo B, Liu T and Yu C 2018 Quantum thermal transistor based on qubit-qutrit coupling *Phys. Rev.* E **98** 022118
[14] Díaz I and Sánchez R 2021 The qutrit as a heat diode and circulator *New J. Phys.* **23** 125006
[15] Segal D and Nitzan A 2005 Spin-boson thermal rectifier *Phys. Rev. Lett.* **94** 034301
[16] Wang C, Ren J and Cao J 2017 Unifying quantum heat transfer in a nonequilibrium spin-boson model with full counting statistics *Phys. Rev.* A **95** 023610
[17] Saito K and Kato T 2013 Kondo signature in heat transfer via a local two-state system *Phys. Rev. Lett.* **111** 214301
[18] Zhang Y, Zhang X, Ye Z, Lin G and Chen J 2017 Three-terminal quantum-dot thermal management devices *Appl. Phys. Lett.* **110** 153501
[19] Majland M, Christensen K S and Zinner N T 2020 Quantum thermal transistor in superconducting circuits *Phys. Rev.* B **101** 184510
[20] Segal D 2006 Heat flow in nonlinear molecular junctions: master equation analysis *Phys. Rev.* B **73** 205415
[21] Senior J, Gubaydullin A, Karimi B, Peltonen J T, Ankerhold J and Pekola J P 2020 Heat rectification via a superconducting artificial atom *Commun. Phys.* **3** 40
[22] Wang C, Chen X M, Sun K W and Ren J 2018 Heat amplification and negative differential thermal conductance in a strongly coupled nonequilibrium spin-boson system *Phys. Rev.* A **97** 052112

[23] Khandelwal S, Perarnau-Llobet M, Seah S, Brunner N and Haack G 2023 Characterizing the performance of heat rectifiers *Phys. Rev. Res.* **5** 013129
[24] Wijesekara R T, Gunapala S D, Stockman M I and Premaratne M 2020 Optically controlled quantum thermal gate *Phys. Rev.* B **101** 245402
[25] Elouard C, Thomas G, Maillet O, Pekola J P and Jordan A N 2020 Quantifying the quantum heat contribution from a driven superconducting circuit *Phys. Rev.* E **102** 030102(R)
[26] Wang L, Wang Z, Wang C and Ren J 2022 Cycle flux ranking of network analysis in quantum thermal devices *Phys. Rev. Lett.* **128** 067701
[27] Ghosh R, Ghoshal A and Sen U 2021 Quantum thermal transistors: operation characteristics in steady state versus transient regimes *Phys. Rev.* A **103** 052613
[28] Wijesekara R T, Gunapala S D and Premaratne M 2021 Darlington pair of quantum thermal transistors *Phys. Rev.* B **104** 045405
[29] Aspelmeyer M, Kippenberg T J and Marquardt F 2014 Cavity optomechanics *Rev. Mod. Phys.* **86** 1391
[30] Rameshti B Z, Kusminskiy S V, Haigh J A, Usami K, Lachance-Quirion D, Nakamura Y, Hu C-M, Tang H X, Bauer G E W and Blanter Y M 2022 Cavity magnonics *Phys. Rep.* **979** 1
[31] Lehnert K W 2014 Introduction to Microwave Cavity Optomechanics *Cavity Optomechanics: Nano- and Micromechanical Resonators Interacting With Light* ed M Aspelmeyer, T Kippenberg and F Marquardt (Springer) pp 233–52
[32] Denis Z, Biella A, Favero I and Ciuti C 2020 Permanent directional heat currents in lattices of optomechanical resonators *Phys. Rev. Lett.* **124** 083601
[33] Xuereb A, Imparato A and Dantan A 2015 Heat transport in harmonic oscillator systems with thermal baths: application to optomechanical arrays *New J. Phys.* **17** 055013
[34] Barzanjeh S, Aquilina M and Xuereb A 2018 Manipulating the flow of thermal noise in quantum devices *Phys. Rev. Lett.* **120** 060601
[35] Yang C, Wei X, Sheng J and Wu H 2020 Phonon heat transport in cavity-mediated optomechanical nanoresonators *Nat. Commun.* **11** 4656
[36] Naseem M T, Misra A, Müstecaplioğlu O E and Kurizki G 2020 Minimal quantum heat manager boosted by bath spectral filtering *Phys. Rev. Res.* **2** 033285
[37] Seif A, DeGottardi W, Esfarjani K and Hafezi M 2018 Thermal management and non-reciprocal control of phonon flow via optomechanics *Nat. Commun.* **9** 1207
[38] Xu H, Mason D, Jiang L and Harris J G E 2016 Topological energy transfer in an optomechanical system with exceptional points *Nature* **537** 80
[39] Zhang K, Bariani F and Meystre P 2014 Quantum optomechanical heat engine *Phys. Rev. Lett.* **112** 150602
[40] Dechant A, Kiesel N and Lutz E 2015 All-optical nanomechanical heat engine *Phys. Rev. Lett.* **114** 183602
[41] Nie W, Li G, Li X, Chen A, Lan Y and Zhu S-Y 2020 Berry-phase-like effect of thermo-phonon transport in optomechanics *Phys. Rev.* A **102** 043512
[42] Clerk A A, Lehnert K W, Bertet P, Petta J R and Nakamura Y 2020 Hybrid quantum systems with circuit quantum electrodynamics *Nat. Phys.* **16** 257
[43] Ockeloen-Korppi C F, Damskägg E, Pirkkalainen J-M, Heikkilä T T, Massel F and Sillanpää M A 2016 Low-noise amplification and frequency conversion with a multiport microwave optomechanical device *Phys. Rev.* X **6** 041024
[44] Barzanjeh S, Vitali D, Tombesi P and Milburn G J 2011 Entangling optical and microwave cavity modes by means of a nanomechanical resonator *Phys. Rev.* A **84** 042342
[45] Xu Q and Blencowe M P 2022 Optomechanical quantum entanglement mediated by acoustic phonon fields *Phys. Rev. Lett.* **129** 203604
[46] Teufel J D, Li D, Allman M S, Cicak K, Sirois A J, Whittaker J D and Simmonds R W 2011 Circuit cavity electromechanics in the strong-coupling regime *Nature* **471** 204
[47] Bernier N R, Tóth L D, Koottandavida A, Ioannou M A, Malz D, Nunnenkamp A, Feofanov A K and Kippenberg T J 2017 Nonreciprocal reconfigurable microwave optomechanical circuit *Nat. Commun.* **8** 604
[48] Gardiner C W and Zoller P 2000 *Quantum Noise* (Springer)
[49] Sekimoto K 2010 *Stochastic Energetics* (Springer)
[50] Ren J, Liu S and Li B 2012 Geometric heat flux for classical thermal transport in interacting open systems *Phys. Rev. Lett.* **108** 210603
[51] Nie W and Lan Y 2012 Thermally driven Casimir ratchet-oscillator system *Phys. Rev.* E **86** 011110
[52] Kosloff R 2013 Quantum thermodynamics: a dynamical viewpoint *Entropy* **15** 2100
[53] Liu Z, Lai Y C and Matias M A 2003 Universal scaling of Lyapunov exponents in coupled chaotic oscillators *Phys. Rev.* E **67** 045203(R)
[54] Lü L, Li C, Liu S, Wang Z, Tian J and Gu J 2015 The signal synchronization transmission among uncertain discrete networks with different nodes *Nonlinear Dyn.* **81** 801
[55] DeJesus E X and Kaufman C 1987 Routh-Hurwitz criterion in the examination of eigenvalues of a system of nonlinear ordinary differential equations *Phys. Rev.* A **35** 5288
[56] Vitali D, Gigan S, Ferreira A, Böhm H R, Tombesi P, Guerreiro A, Vedral V, Zeilinger A and Aspelmeyer M 2007 Optomechanical entanglement between a movable mirror and a cavity field *Phys. Rev. Lett.* **98** 030405
[57] Wilson-Rae I, Nooshi N, Zwerger W and Kippenberg T J 2007 Theory of ground state cooling of a mechanical oscillator using dynamical backaction *Phys. Rev. Lett.* **99** 093901
[58] Marquardt F, Chen J P, Clerk A A and Girvin S M 2007 Quantum theory of cavity-assisted sideband cooling of mechanical motion *Phys. Rev. Lett.* **99** 093902
[59] Liu Y-C, Xiao Y-F, Luan X S and Wong C W 2013 Dynamic dissipative cooling of a mechanical resonator in strong coupling optomechanics *Phys. Rev. Lett.* **110** 153606
[60] Bardeen J and Brattain W H 1948 The transistor, a semi-conductor triode *Phys. Rev.* **74** 230
[61] Bardeen J and Brattain W H 1949 Physical principles involved in transistor action *Phys. Rev.* **75** 1208
[62] Boylestad R L and Nashelsky L 2012 *Electronic Devices and Circuit Theory* 11th edn (Prentice Hall)
[63] Poulsen K, Santos A C and Zinner N T 2022 Quantum wheatstone bridge *Phys. Rev. Lett.* **128** 240401
[64] Bakmou L, Daoud M and ahl laamara R 2020 Multiparameter quantum estimation theory in quantum gaussian states *J. Phys. A: Math. Theor.* **53** 385301
[65] Pinel O, Fade J, Braun D, Jian P, Treps N and Fabre C 2012 Ultimate sensitivity of precision measurements with intense Gaussian quantum light: a multimodal approach *Phys. Rev.* A **85** 010101(R)
[66] Šafránek D 2019 Estimation of Gaussian quantum states *J. Phys. A: Math. Theor.* **52** 035304

[67] Peng J-X, Zhu B, Zhang W and Zhang K 2024 Estimation theory of photon-magnon coupling strength in a driven-dissipative double-cavity-magnon system *Phys. Rev.* A **109** 022601
[68] Leonhardt U 2005 *Measuring the Quantum State of Light* (Cambridge University Press)
[69] Sanavio C, Bernád J Z and Xuereb A 2020 Fisher-information-based estimation of optomechanical coupling strengths *Phys. Rev.* A **102** 013508
[70] Montenegro V, Genoni M G, Bayat A and Paris M G A 2020 Mechanical oscillator thermometry in the nonlinear optomechanical regime *Phys. Rev. Res.* **2** 043338
[71] Li J, Zhu S-Y and Agarwal G S 2018 Magnon-photon-phonon entanglement in cavity magnomechanics *Phys. Rev. Lett.* **121** 203601
[72] Shen R-C, Li J, Fan Z-Y, Wang Y-P and You J Q 2022 Mechanical bistability in Kerr-modified cavity magnomechanics *Phys. Rev. Lett.* **129** 123601
[73] El Anouz K, El Allati A and Metwally N 2020 Different indicators for Markovian and non-Markovian dynamics *Phys. Lett.* A **384** 126122
[74] Zhao X 2019 Macroscopic entanglement in optomechanical system induced by non-Markovian environment *Opt. Express* **27** 29083
[75] Yang X, Yin H, Zhang F and Nie J 2023 Macroscopic entanglement generation in optomechanical system embedded in non-Markovian environment *Laser Phys. Lett.* **20** 015205